

Fermionic Dark Matter Spikes: origin and growth of black hole seeds

Valentina Crespi,^{1,2,*} Carlos R. Argüelles,^{1,2,3,†} and Jorge A. Rueda^{3,4,5,6,7,‡}

¹*Instituto de Astrofísica de La Plata, UNLP-CONICET,
Paseo del Bosque s/n B1900FWA La Plata, Argentina*

²*Facultad de Ciencias Astronómicas y Geofísicas, UNLP,
Paseo del Bosque s/n B1900FWA La Plata, Argentina*

³*ICRANet, Piazza della Repubblica 10, I-65122 Pescara, Italy*

⁴*ICRANet-Ferrara, Dip. di Fisica e Scienze della Terra,
Università di Ferrara, Via Saragat 1, I-44122 Ferrara, Italy*

⁵*ICRA, Dipartimento di Fisica, Sapienza Università di Roma, Piazzale Aldo Moro 5, I-00185 Rome, Italy*

⁶*Dipartimento di Fisica e Scienze della Terra, Università di Ferrara, Via Saragat 1, I-44122 Ferrara, Italy*

⁷*INAF, Istituto di Astrofisica e Planetologia Spaziali,
Via Fosso del Cavaliere 100, 00133 Rome, Italy*

(Dated: December 25, 2024)

We characterize the overdensity (*spike*) of fermionic dark matter (DM) particles around a supermassive black hole (SMBH) within a general relativistic analysis. The initial DM halo distribution is obtained by solving the equilibrium equations of a self-gravitating system of massive fermions at a finite temperature, according to the Ruffini-Argüelles-Rueda (RAR) model. The final fermionic DM spike is calculated around a Schwarzschild SMBH. We explore two possible interpretations for the origin and evolution of the SMBH seed. One corresponds to the traditional scenario proposed by Gondolo & Silk (1999), where a small BH mass of baryonic origin sits at the halo's center and grows adiabatically. The other one, from DM origin, where the dense and degenerate fermion core predicted by the RAR model grows adiabatically by capturing baryons until its gravitational collapse, providing a heavy SMBH seed, whose specific value depends on the fermion mass. We study different initial fermionic DM profiles that the theory allows. We show that overall dilute (i.e., Boltzmannian) fermionic DM develops the well-known spike with density profile $\rho \sim r^{-3/2}$. Instead, for semi-degenerate fermions with a dense and compact core surrounded by a diluted halo, we find novel spike profiles that depend on the particle mass and nature. In the more general case, fermionic spikes do not develop a simple power-law profile. Furthermore, the SMBH does not always imply an enhancement of the surrounding DM density; it might also deplete it. Thus, the self-consistent inclusion of the DM candidate nature and mass in determining the structure and distribution of DM in galaxies, including the DM spikes around SMBHs, is essential for the specification of DM astrophysical probes such as BH mergers, gravitational waves, or stellar orbits.

Keywords: Dark matter(353) — Galactic center(565) — Schwarzschild black holes(1433)

I. INTRODUCTION

Since the past two decades, it has been well established that dark matter (DM) particles may conglomerate around a central black hole (BH), forming an overdensity in the local surroundings [1–4]. The first heuristic calculations were aimed at baryonic matter cusps, by computing the density of a star cluster near a collapsed object, assuming a distribution function given by a power law in the star's energy [5]. Later on in Young [6], it was developed a numerical model based on radial action conservation of the stars, recovering Peeble's main result. There, at the center of the embedding distribution ($\rho_i \sim r^{-2}$), a density cusp was obtained with $\rho_f \sim r^{-3/2}$. This work was later extended by [7] with the adoption of the isochrone model [8] as an example of models with analytic cores, different than the isothermal law, and γ -models [9] for non-analytic cores. They derived a relation

for the initial and final slope of the density distribution by scaling relations of the particle's energy and radii, and imposing total mass and angular momentum conservation.

Gondolo and Silk [1] (hereafter G&S) applied these seminal ideas to DM halos with initial power-law cusps as suggested by N-body simulations. They explored different initial power-law DM distributions $\rho_i(r) \propto r^{-\gamma}$ with $0 < \gamma < 2$, coining for the resulting central over-densities $\rho_f(r) \propto r^{-\gamma_{sp}}$ with $2.25 < \gamma_{sp} < 2.5$, the name of DM spikes. Like their predecessors, the resulting DM density spike was calculated in the Newtonian regime. However, G&S assumed *ad-hoc* integration limits to incorporate the effects of gravitational capture of the central BH. This resulted in an inner (starting) radius for the DM density, given by $4R_{\text{sch}}$, where R_{sch} is the Schwarzschild radius. In Sadeghian *et al.* [4] such an approximation was improved by using a general relativistic treatment leading to an innermost boundary radius of $2R_{\text{sch}}$, with consequent higher densities for the DM spike.

With the aim to reach a more realistic description of DM spikes than obtained in G&S, several studies have remarked that DM overdensities at galactic centers may

* Contact author: valentinacrespi@fcaglp.unlp.edu.ar

† carguelles@fcaglp.unlp.edu.ar

‡ jorge.rueda@icra.it

be attenuated by dynamical processes and different initial conditions for the BH growth. Some examples are off-centered BH seeds, mergers of the host galaxies, and baryon adiabatic contraction [2, 3, 10, 11]. More generally, open problems such as the origin, location, and mass of the initial BH-seed and the consequent time-scale needed to reach a given spike, are recently started to be addressed within specific BH-formation scenarios in a cosmological framework [12]. It is thus the aim of this paper to cover some of these open issues for fermionic DM profiles within a fully relativistic treatment, providing key insights into the nature and mass of the DM particle and possible origin and growth of the initial BH-seeds. The need for such a more realistic treatment aimed at galaxy centers, is justified by different indirect DM searches; gravitational waves (GWs) detection; or even to better understand the motion of stars in its surroundings.

In particular, the center of the Milky Way galaxy has been one of the most attractive targets for indirect searches of DM. If DM particles self-interact, these enhancements should lead to potentially detectable fluxes of high-energy radiation emanating from the central regions [13, 14]. Many projects and experiments have been developed to constrain the DM annihilation and decaying rates, and to model the emission coming from the galactic center [15–18]. Likewise, observations of S-cluster stars around SgrA* were used to put constraints on the size and mass of the spike [19–22]. DM spikes could also be a relevant target for GWs detectors [23]. In principle, detecting and characterizing DM spikes around BHs is feasible by measuring their influence on the gravitational waveform during BH mergers [24–27]. However, from the observational viewpoint, there is yet no definitive evidence either in favor or against the existence of DM density enhancements at the center of galaxies.

At this point, it is worth recalling that the self-consistent inclusion of the DM nature and mass in the determination of the behavior, structure, and distribution of DM in galaxies, including the DM spikes around SMBHs, is essential for the specification of DM astrophysical probes or the analysis of observational data. This paper aims to characterize the DM spikes around SMBHs in the case DM particles are massive, neutral fermions. For this task, we apply the general relativistic approach derived in [4] and adopt as the initial DM halo the equilibrium configurations of self-gravitating fermions, obtained with the extended Ruffini-Argüelles-Rueda (RAR) model [28, 29]. Our motivation to work under such a fermionic DM context is (at least) twofold. First, the very particles (i.e. massive $\mathcal{O}(10^1 - 10^2)$ keV fermions) conforming our DM halos are in agreement with the large scale structure of the Universe as well as the DM halo formation [30]. Indeed, in that work it was demonstrated that in a non-linear structure formation theory based on a Maximum Entropy Production Principle for fermions, the most general solution is stable and develops a degenerate compact core surrounded

by a diluted halo. Such core-halo density profile explains a variety of galactic observables, e.g., the flatness of the outer halo rotation curves [29, 31], the phase-space data of the GD-1 stellar stream [32], galaxy universal relations [31, 33], and the motion of the innermost stars near the Milky Way’s center [34–36]. Thus, it provides a novel kind of DM profile which resembles the ones obtained in N-body simulations in the outer halo [31], but at the center it develops a highly dense core which has never been analyzed in the context of DM spikes once a central BH-seed is formed.

Second, the DM massive fermions have an additional astrophysical and cosmological appeal: under given conditions and for a given particle mass, the dense DM core becomes unstable against gravitational collapse, forming a SMBH at a well-established critical mass which is still surrounded by the halo [30, 37, 38]. Thus, this fermionic theory provides a novel mechanism for SMBH formation in terms of DM, with key applications to the open problem of origin and SMBH seeds in the high redshift Universe [38]. In particular, the collapse of cores made of, let say $m = 100$ keV fermions, form SMBHs of $M_{\text{BH}} = 6.3 \times 10^7 M_{\odot}$. The heavier the fermion, the lighter the SMBH. Starting from these heavy BH seeds, SMBHs of even a few $10^9 M_{\odot}$ can form in less than a Gyr by accreting baryonic matter at sub-Eddington rates [37].

Further, Argüelles *et al.* [38] showed that the sedimentation of ordinary matter (e.g., by accretion or galaxy mergers) at the bottom of the dense DM core triggers its gravitational collapse at a lower critical mass, that can be up to $\approx 40\%$ of the critical mass of a pure DM core. The above baryon-induced collapse scenario for SMBH formation, strongly motivates exploring the consequences of this novel SMBH formation channel at the cosmological and galactic levels. Indeed, regarding the high redshift Universe, as shown in [38], it could explain the unexpectedly observed population of SMBHs in the early Universe by the James Webb Space Telescope [39–41]. On galaxy scales, the application of the above framework is one of the main focus of this paper, which assesses how the fermionic DM density profile reacts over the course of evolution due to the presence of a newly formed SMBH at its center. Two different scenarios about the nature, origin and evolution of the central BHs will be considered as detailed in Sec. III.

The outline of this work consists of describing the theoretical framework to obtain the fermionic DM mass density in section II, together with a description of the fermionic DM model within the RAR theory, including its relevance in the process of formation of central SMBHs recently shown in Argüelles *et al.* [38]. Section III presents the results for several fermionic DM overdensities, depending on the nature of the BH-seed considered, and contrast the obtained spikes with previous ones in the literature. In section IV, we summarize the results of this work, including the current limitations of the theoretical framework and possible extensions, as well as potential applications to be further analyzed in forth-

coming research. Appendix A details the use of adiabatic invariants to relate particle's energies, and appendix B develops on the calculation to obtain the distribution of DM when a SMBH suddenly appears in the center.

II. THEORETICAL FRAMEWORK

A. Relativistic framework

We consider the seminal work by G&S for the calculation of the particle density profile after a central SMBH is adiabatically formed in the center of a DM halo. Specifically, we follow the fully relativistic treatment of this procedure generalized by [4, sec.III] for the growth of a Schwarzschild BH.

For a statistical description of an array of particles, we can write the mass current four-vector as a first moment (in p^μ/m) of the distribution function (DF) $f(\mathbf{x}, \mathbf{p})$ [42, Ch.IV]

$$J^\mu(\mathbf{x}) = \int f(\mathbf{x}, \mathbf{p}) \frac{p^\mu}{m} \sqrt{-g} d^4p, \quad (1)$$

where m is the particle's rest mass, p^μ the four momentum and g is the determinant of the metric. We hereafter adopt geometric units $c = G = 1$, but restore to astrophysical units in the quantitative examples.

The metric of the spherically symmetric Schwarzschild spacetime for a BH of mass M_{BH} is

$$ds^2 = g_{00}(r)dt^2 + g_{11}(r)dr^2 - r^2d\theta^2 - r^2\sin\theta d\phi^2, \quad (2a)$$

$$g_{00}(r) = -g_{11}(r)^{-1} = \left(1 - \frac{2M_{\text{BH}}}{r}\right). \quad (2b)$$

To account for the BH capture effects, it is convenient to change variables from p^μ to constants of motion, making explicit the dependence on the particle's angular momentum, L . Any particle with $L < L_{\text{cr}} = 2\sqrt{3} M_{\text{BH}}$ will cross the BH horizon. The mass density, related with the mass current by $\rho(r) = \sqrt{g_{00}(r)}J^0$, becomes

$$\rho(r) = \frac{4\pi m^4}{r^2 \sqrt{g_{00}}} \int_{\mathcal{E}_1}^{\mathcal{E}_2} \mathcal{E} d\mathcal{E} \int_{L_1}^{L_2} \frac{f(\mathcal{E}, L) L dL}{\sqrt{\mathcal{E}^2 - g_{00}(1 + \frac{L^2}{r^2})}}, \quad (3)$$

where \mathcal{E} and L are the particle's conserved (along the geodesic) energy and angular momentum per unit rest mass. As the integrals are computed for every radial position r , the integral limits need to have this explicit dependence. With a study of the particle's radial motion, its effective potential $\mathcal{V}_{\text{eff}}^2(r, L) = g_{00}(r)(1 + L^2/r^2)$, and

considering only bound orbits, we find these limits

$$(L_1)^2 = \frac{27\mathcal{E}^4 - 36\mathcal{E}^2 + 8 + \mathcal{E}(9\mathcal{E}^2 - 8)^{3/2}}{2(\mathcal{E} - 1)}, \quad (4)$$

$$(L_2)^2 = r \left(\frac{\mathcal{E}^2}{g_{00}(r)} - 1 \right), \quad (5)$$

$$\mathcal{E}_1 = \begin{cases} (1 - 2/r)/\sqrt{1 - 3/r}, & 4 \leq r/M_{\text{BH}} \leq 6, \\ (1 + 2/r)/\sqrt{1 + 6/r}, & r/M_{\text{BH}} \geq 6, \end{cases} \quad (6)$$

$$\mathcal{E}_2 = 1. \quad (7)$$

Equation (4) corresponds to the maximum of \mathcal{V}_{eff} achieved when $\mathcal{V}_{\text{eff}}(r_1, L_1) = \mathcal{E}$ (r_1 is the location of the maximum, i.e., $d\mathcal{V}_{\text{eff}}/dr = 0$, $d^2\mathcal{V}_{\text{eff}}/dr^2 < 0$) and is equivalent to Eq. (3.16) in Sadeghian *et al.* [4]. Equation (5) corresponds to the inner turning point $\mathcal{V}_{\text{eff}}(r, L) = \mathcal{E}$ ($\dot{r} = 0$), and Eq. (6) to energies equal to the maximum of the effective potential, $\mathcal{V}_{\text{eff}}(r, L_1(\mathcal{E}_1)) = \mathcal{E}_1$, and solving for \mathcal{E}_1 .

The DF in eq. (3), $f(\mathcal{E}, L)$, which describes the distribution of DM particles under the influence of the grown BH, is *a priori* unknown. However, under the assumption of adiabatic growth of the initial BH-seed, the final form of the DF can be related to the known initial DF for particles orbiting in a self-gravitating DM halo. This approach is valid when the changes in the BH gravitational potential occur on slow timescales compared to dynamical periods of particles in regions where the BH dominates. The BH gravitational influence radius can be estimated as $R_{\text{inf}} = c^2 R_{\text{sch}}/2\sigma^2 \sim 10^6 R_{\text{sch}}$, where σ is a typical velocity dispersion dictated by the BH's gravitational potential [43, Ch. 3.6]. Indeed, this is the case for central orbits in a galaxy with periods $t_{\text{dyn}} \lesssim R_{\text{inf}}/\sigma \sim 10^4$ yr. In turn, the SMBH growth timescale assuming Eddington-limited accretion is $t_{\text{BH}} = M_{\text{BH}}/\dot{M} \sim 10^7$ yr.

Thus, over the course of this adiabatic growth, the action variables of the particles remain constant, allowing us to relate the initial and final states in energy and angular momentum of the DM orbits. In appendix A, we present the numerical computation of this relation. We apply this formalism in: i) a negligible BH-seed adiabatically growing in the center of a fermionic RAR halo, namely Model I (see Sec. III A), and ii) a DM fermion-core accreting baryons and hence, adiabatically growing to its critical state for gravitational collapse, corresponding to Model II (as detailed in Sec. III B).

B. Fermionic DM halos: extended RAR model

It describes self-gravitating, neutral, spin 1/2, massive fermions in hydrostatic and thermodynamic equilibrium within the GR framework. The equation of state of the DM particles' perfect fluid accounts for the tidal truncation of particles with large momenta through a cutoff parameter. The DF is dictated by a Fermi-Dirac-like function, which, under spherical symmetry, is given in

space of energies by

$$f(\mathcal{E}) = \frac{2}{h^3} \frac{1 - \exp[(\mathcal{E} - \mathcal{E}_c)/(\sqrt{g_{00}(r)}\beta(r))]}{1 + \exp[(\mathcal{E}/\sqrt{g_{00}(r)} - \alpha(r))/\beta(r)]}, \quad (8)$$

where h is Planck's constant, $g_{00}(r)$ is the 00 component of the metric tensor and \mathcal{E} , $\beta(r)$, $\alpha(r)$ are the particle's total energy, temperature and relativistic chemical potential per unit rest mass m , i.e.,

$$\mathcal{E} = \sqrt{g_{00}(r)}\varepsilon(r), \quad \beta(r) = \frac{k_B T(r)}{m}, \quad \alpha(r) = \frac{\mu(r)}{m}. \quad (9)$$

Equation (8) is equivalent to the DF adopted in other works for self-gravitating fermions in GR [e.g. 29, 30, 33, 34, 44], though in this case written in terms of the (global) particle's energy \mathcal{E} which relates with the usually assumed (local) particle's energy, $\varepsilon = \sqrt{m^2 + p^2}/m$ by eq. (9). The cut-off energy \mathcal{E}_c , sets a limit for tidal truncation ($f(\mathcal{E} > \mathcal{E}_c) = 0$).

It is also convenient to make use of the fermion's degeneracy parameter θ , which corresponds to

$$\theta(r) = \frac{\mu(r)}{k_B T(r)} \quad (10)$$

We recall that the above Fermi-Dirac-like DF results from a maximum entropy production principle for fermions, which was applied within collisionless relaxation process for DM halos in [45–47]. These DM halos are proved to be stable, long-lived and of astrophysical interest as shown for the first time in [30], within a cosmological framework.

The model equilibrium equations consist of the Einstein equations, where the mass-energy source is given by a perfect fluid with (4-parametric) equations of state, together with the Tolman and Klein conditions, which are a generalization of the zero and first laws of thermodynamics in GR (see [48] for an original work, and [49] for a re-derivation in terms of entropy maximization); and a cutoff condition from energy conservation along a geodesic. A more detailed description and the model equations can be found in [29, 30, 33].

The most general solution leads to a DM density radial profile characterized by a nearly homogeneous, degenerate compact core (governed by Pauli degeneracy pressure and highly sensitive to the particle mass), followed by an extended and diluted halo (governed by thermal pressure). Such *dense core–diluted halo* distributions correspond to positive central degeneracies parameter $\theta_0 \gtrsim 10$ constituting the core-halo family of solutions [28, 30]. For low central degeneracy parameter $\theta_0 \ll -1$, we obtain the relativistic analog of the King model of a diluted fermi gas with cutoff (resembling the Burkert DM profile as shown in [31]). Figure 4 shows two RAR-DM halos obtained with high and low central degeneracy parameters ($\theta_0 = -33$ and $\theta_0 = +39$, dotted lines). We recall that this model does not include particle self-annihilation, consistent with the obtained temperatures, which fulfill $T \ll m/k_B$.

C. Baryon-induced collapse: DM cores into SMBHs

As shown in [37], the core-halo solutions following equilibrium configurations as the central density grows, can reach a state of gravitational core-collapse into a SMBH. These critic cores can be well approximated by configurations in the fully degenerate regime, for which the limiting mass is given by the Oppenheimer-Volkoff relation [50]

$$M_{\text{crit}}^{(0)} \approx 0.38 \frac{m_{\text{Pl}}^3}{m^2} = 6.27 \times 10^7 \left(\frac{100 \text{ keV}/c^2}{m} \right)^2 M_{\odot}, \quad (11)$$

where $m_{\text{Pl}} = \sqrt{\hbar c/G} = 2.18 \times 10^{-5} \text{ g}$ is Planck's mass. As detailed in [38], when taking into account the combination of DM + baryonic matter, the new equilibrium configurations with its corresponding turning point sequence in a M Vs. ρ_c plane, lead to a new value of the critical mass for gravitational collapse (achieved when $\partial M/\partial \rho_c = 0$, with ρ_c the central density). This value will depend on the baryonic-to-DM mass fraction $\chi = M_b/M_{\text{dm}}$, that may take values between $0 \leq \chi \leq 0.8$. These new channel of SMBH formation from collapsed cores as heavy seeds, allows SMBHs of a few $10^9 M_{\odot}$ to form in less than 1 Gyr by accreting baryonic matter at sub-Eddington rates.

A possible sequence of events in the baryon-induced collapse framework is as follows: there is a starting core-halo configuration (pure DM, $\chi = 0$) on which the baryonic matter starts to fall into its potential well, modifying its equilibrium state. The total configuration evolves in time, until it reaches the gravitational collapse condition where a SMBH is formed with mass $M_{\text{BH}} = M_{\text{crit}}$ within a fraction of Gyr for typical baryon fraction. For a realistic core collapse via baryonic induction to occur –that is, in $O(t \sim \text{Gyr})$ – there is a minimum DM core mass above which, when accreting baryons, the critical mass is reached. This threshold value is given by

$$M_{\text{dm}}^{(\text{min})} \approx 0.22 M_{\text{crit}}^{(0)} \quad (12)$$

for which it corresponds a maximum SMBH formation time $t_{\text{BH}}^{(\text{max})} = 0.44\tau$, where the timescale τ takes the baryon physics into account

$$\tau \approx 4.21 \left(\frac{M_{\odot}/\text{pc}^3}{\rho_b} \right) \left(\frac{v_b}{100 \text{ km/s}} \right)^3 \left(\frac{10^6 M_{\odot}}{M_{\text{dm}}} \right) \text{ Gyr} \quad (13)$$

where ρ_b is the baryon density at the gravitational capture radius $R_{\text{cap}} = 2GM/v_b^2$, v_b is the baryons speed and $M_{\text{dm}} = M(t=0)$ is the initial mass (pure DM). In the same manner described in section II A, the baryonic induction process occurs in the adiabatic regime, when a DM core with mass $M_{\text{dm}}^{(\text{min})}$ accretes baryons growing (together) to M_{crit} . However, contrasting the SMBH formation from a negligible (adiabatically growing) BH-seed, in this scenario the SMBH formation occurs *instantaneously*, via DM-core collapse.

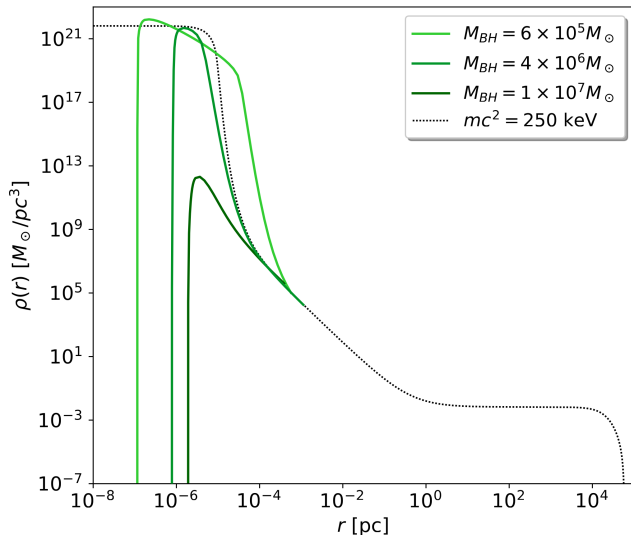


FIG. 1. Mass density profiles in green palette, resulting from adiabatic growth of a central BH with final values of $M_{\text{BH}} = 6 \times 10^5, 4 \times 10^6, 1 \times 10^7 M_{\odot}$ (corresponding to Model I). The black dotted line corresponds to the original DM halo with a fermion mass of $m = 250$ keV.

In section III B we perform an application of this approach. We consider a starting fermionic core-halo distribution of $mc^2 = 300$ keV and $M_{\text{dm}} = 1.5 \times 10^6 M_{\odot}$. For these fermions the Oppenheimer-Volkoff mass is $M_{\text{crit}}^{(0)} = 7 \times 10^6 M_{\odot}$ ($\chi = 0$). Adopting the value $\chi = 0.5$, the corresponding critic mass for collapse, and hence, the resulting SMBH mass is $M_{\text{crit}} = M_{\text{BH}} = 4 \times 10^6 M_{\odot}$. There, we show the results on the re-distribution of this fermionic DM halo surrounding a SMBH that had its origin from a DM core via baryonic induced collapse. In appendix B, we develop on the rearrangement of DM orbits when the gravitational potential suffers a sudden change, from a fermionic compact core to the most compact solution, a Schwarzschild BH.

III. RESULTS

A. Model I: BH growth from baryons

In this interpretation, we computed the dynamical rearrangement of DM particles, assuming an SMBH has grown adiabatically in the center within $\sim 10^7$ yr. We implemented different host DM configurations given by the RAR model, for which the same outer halo is shared, i.e., only differing in the central core compactness (see e.g. [29]). In principle, these general results apply to any size and mass of astrophysical halos [33]. We selected those corresponding to typical Milk Way like galaxies in order to compare with previous results for spikes originated in different DM halo models. To achieve this, we imposed appropriate boundary conditions given

by $M(r = 29 \text{ kpc}) = 1.8 \times 10^{11} M_{\odot}$, a total mass of $M(r_b = 58 \text{ kpc}) = 2.4 \times 10^{11} M_{\odot}$ and a core mass set to $M_c = 3.5 \times 10^6 M_{\odot}$, as in Becerra-Vergara *et al.* [34, 35].

In Fig. 1, we present the spike density profiles that arise in a RAR core-halo configuration, as the central mass of the SMBH grows. In dotted black, the host halo of $m = 250$ keV fermions is shown. These profiles could be seen as the evolution of the DM spike as the BH grows. In particular, for this 250 keV halo, we find that spikes with central BH masses below $\lesssim 4 \times 10^6 M_{\odot}$ show an extended power law behavior in its peak, with index $\gamma = 3/2$. For larger BH masses, the spike becomes sharper but lower.

Figure 2 compares DM spikes formed within three different halos of particle masses $m = 100, 250,$ and 378 keV, for three selected values of the central BH mass, $10^6 M_{\odot}, 4 \times 10^6 M_{\odot},$ and $3 \times 10^7 M_{\odot}$. The same trend of the DM spike evolution holds for all DM particle masses, although the shrinking of the spike highly depends on its value. This behavior is related to the compactness of the original DM core, which increases with the particle mass. Eventually, for sufficiently high BH mass ($\sim 10^7 M_{\odot}$), the DM spikes begin to resemble each other, independently of the particle mass, and tend to the spike predicted by the non-singular isothermal sphere (NSIS) profile (Fig. 2, right panel). The above occurs because, inside the BH sphere of influence ($\sim 10^6 R_{\text{sch}}$), the DM particles that have not fallen in (i.e., with $L > 2\sqrt{3}M_{\text{BH}}$) have a low degeneracy parameter, leading to their behavior in a Boltzmannian regime.

Figure 3 shows the tendency of the maximum density ρ_{max} of the peak of the spike as a function of the BH mass for several fermion masses. The dashed horizontal lines correspond to the central density ρ_0 of the original DM halos. The shrinkage of the peaks occurs earlier as the particle mass increases. For BH masses where the peaks maintain approximately the same height (e.g., 100 keV, black line from $M_{\text{BH}} \lesssim 10^7 M_{\odot}$), is the region of power-law behavior, where the spike profile only changes in its width (see left and middle panels of Fig. 2, 100 keV green lines). Interestingly, at fixed fermion mass, there is a BH mass over which the spike density depletes instead of enhanced relative to its initial value (i.e., compared with the horizontal dashed lines). Furthermore, there is a threshold particle mass, $m_{\text{th}} \sim 300$ keV, above which there is no DM density enhancement for any BH mass.

Figure 4 compares the sizes and scales of three different DM spikes for the same central BH. We set the value to $M_{\text{BH}} = 4 \times 10^6 M_{\odot}$ in order to compare with the spike of G&S and other works. For two of the spikes, we adopt as host halo the RAR model for $m = 100$ keV fermions, differing in the central degeneracy parameter value. For $\theta_0 = 39$, the original profile is of the core-halo family, whereas for $\theta_0 = -33$, the profile is that of (relativistic) NSIS with cutoff. For the remaining spikes, we adopt as the original DM halo a power-law density model with index r^{-1} , corresponding to the inner region of a Navarro-Frenk-White (NFW) DM halo [51]. We con-

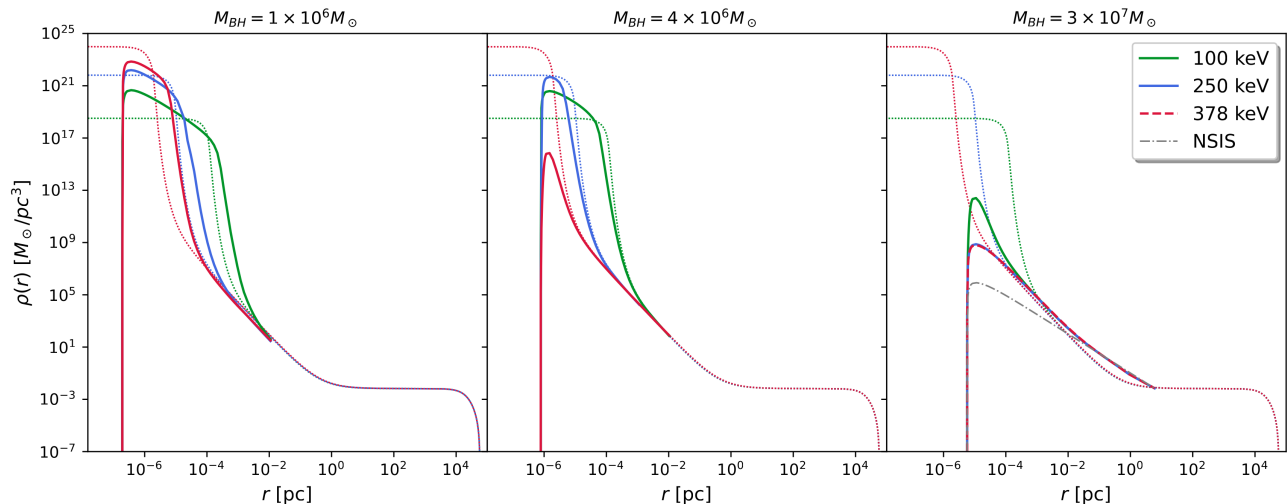


FIG. 2. Density profiles corresponding to original DM halos with fermion masses of $m = 100, 250, 378$ keV. The original configurations are represented in dotted lines, while the resulting spikes are in solid lines. As the central BH mass increases, the DM spikes change their behavior. (Left) all DM profiles present a power law with $r^{-3/2}$ in its peak. (Middle) the spikes get narrower, and the peaks decrease. The size of this depletion depends on the particle mass. (Right) for a more massive central BH, all spikes start to resemble each other, tending to the Boltzmannian spike for an original NSIS DM profile.

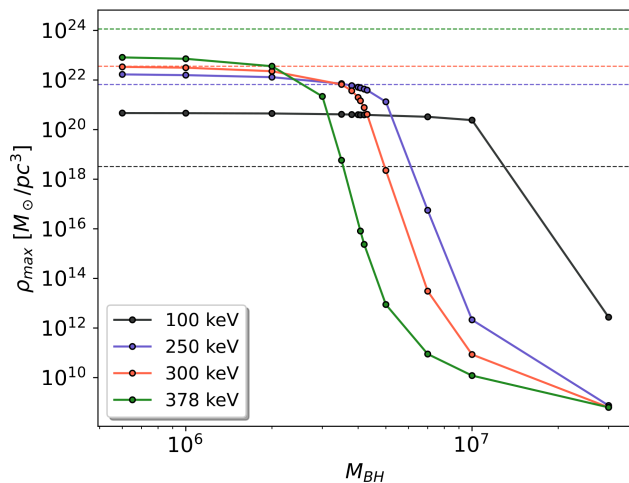


FIG. 3. Dependence of the peak heights with the central BH mass, ranging from $M_{\text{BH}} = 6 \times 10^5 M_{\odot}$ to $M_{\text{BH}} = 3 \times 10^7 M_{\odot}$, for different DM particle masses. The dashed horizontal lines correspond to the values of central densities of the original DM halos. See also Figure 2 for selected spikes with given central M_{BH} values.

sider in this case, for the sake of comparison with G&S, a minimum value for the angular momentum given by $L_c = 2R_{\text{sch}}$, which leads to a spike vanishing at $4R_{\text{sch}}$ instead of $2R_{\text{sch}}$. We adopt as well, the spike obtained in the fully relativistic treatment computed in [52]. It is worth noticing that, for RAR configurations with low central degeneracies (where the fermions behave in

a Boltzmannian regime), we recover the spike found by G&S and other authors, where the density goes with $r^{-3/2}$, as expected for models with finite cores (Fig 4, blue lines). A first observation to be drawn from these results is that, although higher spike peaks are found with RAR host halos, the DM overdensity is always in a narrower region of radius, as compared to spikes arising from power-law profiles which are lower but more widespread.

B. Model II: DM core collapse

In this approach, we combine the two formalisms detailed in sections II A and II C. We separate the problem in two stages:

i) We start with an initial (sub-critic) core-halo equilibrium configuration. The DM core, of mass $M_{\text{dm}} \geq M_{\text{dm}}^{(\text{min})}$, accretes baryons and consequently grows to its critical mass for gravitational collapse, M_{crit} . The timescale on which this occurs is $\sim 0.1\text{--}1$ Gyr [38]. Therefore, the core grows in the adiabatic regime.

ii) Once the compact core has reached the critical mass, the gravitational collapse of the core sets in. All the particles belonging to the core collapse into an SMBH. The remaining particles orbit in a new, suddenly changed gravitational potential.

To illustrate this method, we selected an initial equilibrium configuration for $mc^2 = 300$ keV fermions, with a core of mass $M_{\text{dm}} = 1.5 \times 10^6 M_{\odot}$. The baryonic to DM mass fraction at the time of collapse is $\chi = 0.5$, with corresponding critic mass $M_{\text{crit}} = 4 \times 10^6 M_{\odot}$ according to the baryon-induced collapse scenario [38]. In-

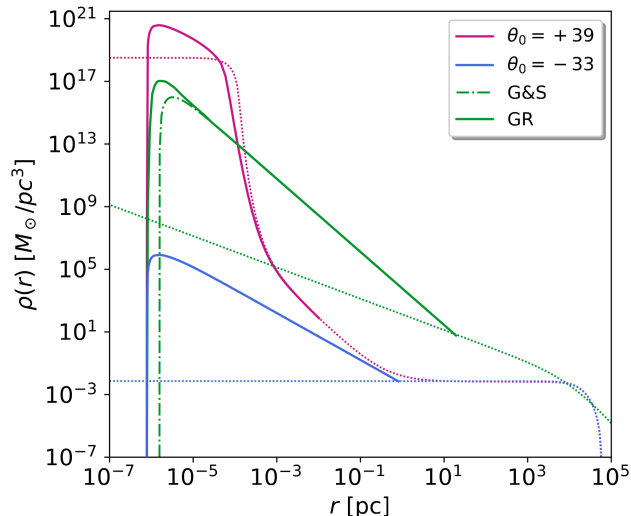


FIG. 4. Density profiles corresponding to original DM halos with fermion mass of $m = 100$ keV. In purple for a core-halo solution with a high central degeneracy parameter of $\theta_0 = 39$, in blue for a low central degeneracy solution with $\theta_0 = -33$, corresponding to the Boltzmannian regime. For comparison, the DM spike of G&S is shown in dotted-dashed green line, and its relativistic correction in solid green (the latter was adapted from [52]). These spikes are obtained from a typical NFW halo, shown in dotted green. The chosen central BH mass in all cases is $M_{\text{BH}} = 4 \times 10^6 M_\odot$, to contrast with other works.

stead, the pure DM critic core ($\chi = 0$) corresponds $M_{\text{crit}}^{(0)} = 7 \times 10^6 M_\odot$. In figure 5 we show the evolutionary process, according to model II, of the core-halo DM profile. For the first stage, we perform the numeric computation of the new DM density using equation 3, where $g_{00}(r)$ now corresponds to the metric produced by the compact critic core M_{crit} (see figure 8), and the integration limits in \mathcal{E} and L correspond to a regular distribution. As expected, we found the redistribution of DM particles closely resembling that of a core-halo profile in which the core is critic (see figure 5, stage 1). When the core suffers a (radial) gravitational collapse, the remaining DM particles suffer a change in energy, which leads to orbits with inner pericenters, these limited by $2R_{\text{Sch}}$ (see figure 5, stage 2). In figure 6, we compare the resulting spikes given by models I and II, for the same value of central M_{BH} , and same core-halo host DM profile. We find these results with a slight difference, showing up only at the peak. The flattening of the peak in model II, corresponds to the subtraction of DM particles that belonged to the core at the time of collapse. The details of this numeric computation are shown in Appendix B.

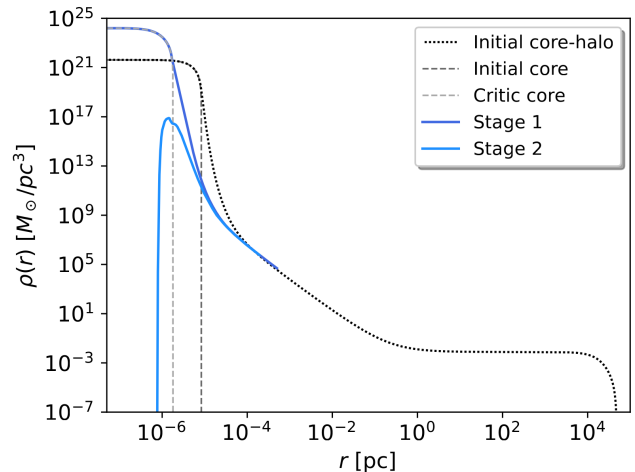


FIG. 5. Evolutionary process of a core-halo DM configuration of 300 keV fermions (dotted black). In stage 1, the central core (initial core, dashed gray) adiabatically grows as it accretes baryons, until it reaches the critic mass for gravitational collapse (critic core, dashed dotted gray). Consequently, the particles re-accommodate under the core central potential (solid dark blue). The critic values are $M_{\text{crit}} = 4 \times 10^6 M_\odot$ and a baryon to DM mass fraction of $\chi = 0.5$. After collapse is triggered, a SMBH is formed with $M_{\text{BH}} = M_{\text{crit}}$ and the remaining DM forms a spike density shown in solid blue.

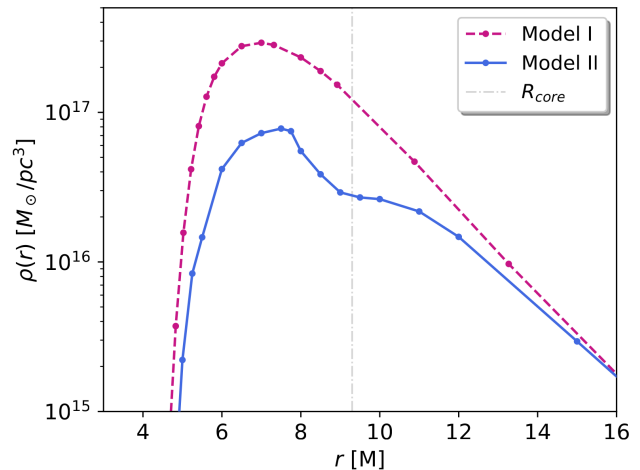


FIG. 6. Comparison of spike profiles for the same central $M_{\text{BH}} = 4 \times 10^6 M_\odot$, formed in a core-halo DM configuration of 300 keV fermions. In model I, the DM particles rearrange around an adiabatically growing BH (dashed purple). In model II, the remaining DM particles conform the spike density profile, after core collapse into a SMBH (solid blue). The critical core radius is $R_{\text{core}} = 9.3 M_{\text{crit}}$.

IV. DISCUSSION AND CONCLUSIONS

Much is being discussed in the literature on the theoretical prediction that DM around BHs enhances its density, forming the so-called DM spikes. Specifically, it

has been widely adopted that the density profile of such DM spikes obeys a power-law behavior. In this work, we have calculated the density spikes of DM made of massive, neutral fermions within a general relativistic analysis. We have obtained the initial DM profiles within the RAR model framework, which adopts the fermion gas at finite temperatures in hydrostatic and thermodynamic equilibrium (see section II B). We assess different states of central degeneracy of the fermions, as well as different particle masses. We have adopted two possible interpretations for the BH-seed origin and evolution, namely Model I and II. In the former, the spikes theoretical treatment follows a relativistic extension of the G&S method, detailed in section II A and appendix A. In this framework, the spikes are formed and evolve adiabatically within a self-gravitating DM halo, from a negligible BH seed (possibly of baryonic origin). The key results are:

1. Given a central M_{BH} , the fermionic spike density profile crucially depends on the mass of the DM particles and their physical regime (state of degeneracy). Instead, for power-law DM halos, the resulting spike density profile only depends on the value of the initial power-law index γ .
2. We have shown that the DM spikes arising by fermionic core-halo configurations, do not develop a simple power-law profile (see, e.g., figs. 1 and 2).
3. For a given fermion mass, there is a specific mass of the central BH above which there is no density enhancement, but on the contrary, it decreases relative to the initial one (see fig. 3). Moreover, for fermion masses above ~ 300 keV, there is no enhancement of the density of the DM surrounding the BH for any BH mass, but a suppression.
4. The typically assumed power-law DM spikes occur only in the case of initial DM configurations in the Boltzmannian regime. In the RAR case when the central fermions are in a state of low degeneracy ($\theta_0 \ll -1$), we recover the resulting DM spike of $\rho \propto r^{-3/2}$ typical of cored halos as the NSIS (see fig. 4).

If one could constrain the DM distribution at $r \lesssim 1$ kpc scales, given different astrophysical observables, these results would imply an indirect way to predict whether RAR-DM halos are born in a core-halo regime ($\theta_0 \gg 1$), or only as a diluted halo ($\theta_0 \ll -1$).

It is important to recall that this theoretical treatment has some limitations or approximations. In particular, the G&S method strictly speaking, requires that in the initial state, the DM halo is self-gravitating. However once the BH has grown, the gravitational influence of the DM particles is purely due to the BH, and the gravitational potential of the remaining DM mass is neglected. For RAR-DM halos, the enclosed mass inside the grown BH's sphere of influence ($\sim 10^6 R_{\text{sch}}$) will depend on the

fermion mass, in addition to the central M_{BH} mass. For fermions of $mc^2 \lesssim 250$ keV and $M_{\text{BH}} \lesssim 4 \times 10^6 M_{\odot}$, the enclosed mass is comparable to that of the central BH, $M_{\text{DM}} \sim M_{\text{BH}}$. This fact favors the RAR spike profiles with fermion mass of $\gtrsim 300$ keV.

Further requirements for the DM halo are, spherical symmetry, and the BH seed can not be off-center [2, 53].

Regarding Model II, it encompasses a new and fully self-consistent interpretation for the problem of how SMBHs form and evolve at the center of DM halos from a cosmological viewpoint. In this, violent relaxation processes predict that DM fermions can describe spherical distributions in thermodynamic equilibrium, where the most general morphology is a degenerate compact core surrounded by a diluted halo. These core-halo DM profiles are stable (i.e., local maxima of entropy) and extremely long-lived. For these DM halos, there exists a critical point at the onset of instability where the core collapses towards a SMBH. This gravitational collapse can only occur for halo's virial masses of $M_{\text{vir}} \gtrsim 10^9 M_{\odot}$, starting at early universe stages $z_{\text{vir}} \approx 10$ [30]. Furthermore, for DM cores that are not in a critical state (i.e. $\partial M_c / \partial \rho_c = 0$), the collapse can still be triggered by baryonic accretion in a fraction of a Hubble time, producing heavy seeds of DM origin for SMBHs at galactic centers [38]. In this approach, we have calculated the redistribution of the remaining fermionic DM particles, after the critic core had collapsed. The same key findings (1, 2 and 3 of this discussion) apply for this method. However, one difference in point 1 is that the morphology of the fermionic DM spike now depends on the value of the fraction of baryons χ , in addition to the mass of the fermion and its state of degeneracy (for a given central M_{BH}).

The current theoretical framework can be applied to various DM astrophysical probes. In particular, the enhancement of the DM density can have a relevant impact, among others, on stellar dynamics (e.g., stars orbiting BHs), the rate at which a BH grows by accreting DM, and the dynamical friction of DM particles on the motion of BHs in binaries. The latter effect can be particularly important in the analysis of the so-called *final parsec problem* of merging SMBHs. Here, we have focused on the DM spikes around BHs of large masses. It remains an interesting topic to assess whether or not DM also forms spikes around stellar-mass BHs or compact stars like neutron stars. This topic, which has hardly been addressed, is especially relevant for the analysis of the possible role of DM in low-mass and high-mass X-ray binaries [54, 55].

ACKNOWLEDGMENTS

This work used computational resources from CCAD – Universidad Nacional de Córdoba (<https://ccad.unc.edu.ar/>), which are part of SNCAD – MinCyT, República Argentina. V. Crespi thanks financial support from CONICET, Argentina.

Appendix A: Energy relation

Consider stationary and spherical space-times where the line element is given by

$$ds^2 = g_{00}(r)dt^2 + g_{11}(r)dr^2 - r^2 d\theta^2 - r^2 \sin\theta d\phi^2 \quad (\text{A1})$$

A massive test particle in free-fall on this geometry possesses four Killing vectors that lead to conserved quantities, namely the energy per unit rest mass \mathcal{E} , and the three components of the angular momentum per unit rest mass L_x, L_y, L_z .

In the space of angle-action variables, the actions are

$$I_\phi(L_z) = \frac{1}{2\pi} \oint L_z d\phi \quad (\text{A2})$$

$$I_\theta(L, L_z) = \frac{1}{2\pi} \oint \sqrt{L^2 - \frac{L_z^2}{\sin^2(\theta)}} d\theta \quad (\text{A3})$$

$$I_r(\mathcal{E}, L) = \frac{1}{2\pi} \oint \dot{r} dr \quad (\text{A4})$$

where the radial velocity is given by

$$\dot{r}^2 = \frac{\mathcal{V}_{\text{eff}}^2(r, L) - \mathcal{E}^2}{g_{00}(r)g_{11}(r)} \quad (\text{A5})$$

and the form of the effective potential is

$$\mathcal{V}_{\text{eff}}^2(r, L) = g_{00}(r) \left(1 + \frac{L^2}{r^2} \right) \quad (\text{A6})$$

in the case of a Schwarzschild BH we have $g_{00}(r)g_{11}(r) = -1$. The azimuthal action A2 becomes trivially $I_\phi = L_z$, the latitudinal action A3 is $I_\theta = L - L_z$ and the radial action becomes

$$I_r(\mathcal{E}, L) = \frac{1}{\pi} \int_{r_p}^{r_a} \sqrt{\frac{\mathcal{V}_{\text{eff}}^2(r, L) - \mathcal{E}^2}{g_{00}(r)g_{11}(r)}} dr \quad (\text{A7})$$

where r_p and r_a are the pericenter and apocenter of the orbit, respectively. Suppose the central potential in which the particles are confined varies *slowly*, i.e., when the SMBH grows on a timescale much longer than the dynamical particles timescale. In that case, the actions can be assumed not to change in time, constituting the adiabatic invariants [43]. Due to this conservation, the DF of the system is also conserved between an initial and a final state

$$f_i(\mathcal{E}_i, L_i) = f_f(\mathcal{E}_f, L_f). \quad (\text{A8})$$

Equations (A2) and (A3) imply the conservation of angular momentum $L_i = L_f$, and the invariance of the radial action allows us to numerically relate the original and final energies as $\mathcal{E}_i = \mathcal{E}_i(\mathcal{E}_f, L)$.

For this, we first compute the turning points r_p and r_a as a function of \mathcal{E} and L , achieved for the radii where $\mathcal{E} = \mathcal{V}_{\text{eff}}(\mathcal{E}, L)$ using the python SciPy [56] function `scipy.optimize.brenth`; then we calculate the radial

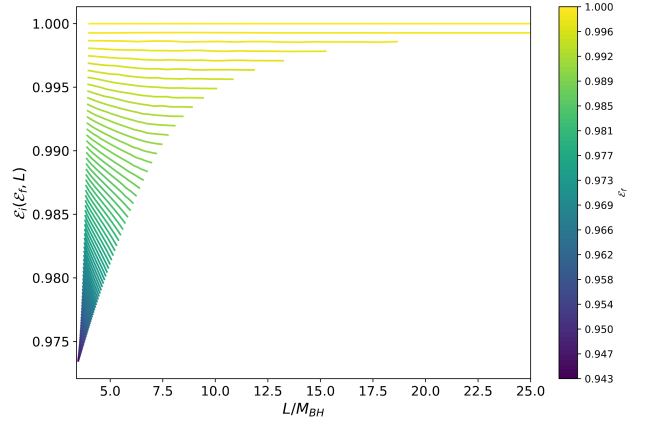


FIG. 7. Color map of the surface of original energies \mathcal{E}_i for DM particles of $m = 250$ keV, as a function of final energies \mathcal{E}_f and angular momentum L for particles orbiting a BH of mass $M_{\text{BH}} = 4 \times 10^6 M_\odot$. The color bar corresponds to final energies \mathcal{E}_f of bound orbits, permitted from $\mathcal{E}_{f,\text{min}} = \sqrt{8/9}$ to $\mathcal{E}_{f,\text{max}} = 1$.

action for every \mathcal{E} , as a function of L , $I_r(L)$ integrating with `scipy.integrate.quad`; and look for the intersections when

$$I_{r,\mathcal{E}_i}(L) = I_{r,\mathcal{E}_f}(L) \quad (\text{A9})$$

This hypersurface in $(\mathcal{E}_i, \mathcal{E}_f, L)$ space is shown in Fig. 7 for the case of an initial DM core-halo configuration for fermions of rest mass $m = 250$ keV, core mass of $M_c = 3.5 \times 10^6 M_\odot$ and central degeneracy of $\theta_0 = 41$.

The range in original energy is $\mathcal{E}_i = [\sqrt{g_{00}(r_0)}, 1]$, where $g_{00}(r)$ corresponds to the fermionic-only metric tensor and $r_0 = 0$; the range in final energy is $\mathcal{E}_f = [\sqrt{8/9}, 1]$, where $\sqrt{8/9}$ corresponds to the lowest possible energy achieved by $L = L_{\text{cr}}$; and the range in angular momentum for every energy is delimited by $L = [L_-(\mathcal{E}), L_+(\mathcal{E})]$, where

$$L_\pm^2(\mathcal{E}) = \frac{27\mathcal{E}^4 - 36\mathcal{E}^2 + 8 \mp \mathcal{E}(9\mathcal{E}^2 - 8)^{3/2}}{2(\mathcal{E}^2 - 1)} M_{\text{BH}}. \quad (\text{A10})$$

These functions correspond to $\mathcal{V}_{\text{eff}}(r_\pm, L_\pm) = \mathcal{E}$ when the energy matches the minimum and maximum of the potential (for r_+, L_+ and r_-, L_- respectively), giving the characteristic shape in Fig. 7.

Finally, to compute the DM density resulting from the adiabatic growth of the central SMBH (Eq. 3), we interpolate the hypersurface using `scipy.interpolate.LinearNDInterpolator` for any of the possible values of \mathcal{E}_f and L ; and perform the double integral with `scipy.integrate.dblquad`.

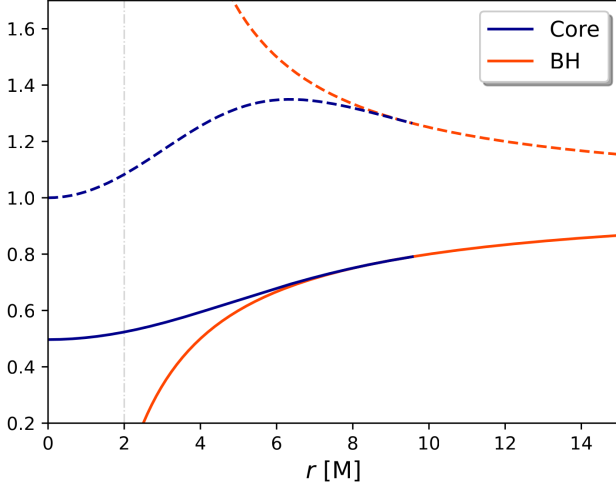


FIG. 8. Metric potentials for the DM critic core in blue and a Schwarzschild BH in red, computed for the same mass $M_c = M_{\text{BH}}$. Solid lines correspond to $g_{00}(r)$ and dashed lines to $-g_{11}(r)$. The core metric, smoothly matches the BH's at the border, $R_c = 9.3 M_c$.

Appendix B: Instantaneous BH collapse

We compute the new orbits of DM particles when the gravitational potential suffers a sudden change as the DM core collapses to a SMBH. This time interval is considered instantaneous compared to the dynamical timescales. We adopt the methodology assumed by [2], where the DM particle conserves its angular momentum L , since the collapse is radial. For a particle located at \mathbf{r}_i with velocity \mathbf{v}_i under the influence of \mathcal{V}_{eff} (eq. A6) before core collapse, its velocity remains unchanged $\mathbf{v}_i(r_i) = \mathbf{v}_f(r_i)$ right after collapse when the potential corresponds to eq. A6 with $g_{00}(r) = 1 - 2M_{\text{BH}}/r$. In figure 8, we show the difference in the metric potentials between the regular critic core, and a Schwarzschild singular solution. Since we want to perform the calculation for a general kind of (bound) keplerian orbit, it is convenient to use the particles's energy and angular momentum, as done in [12]. The probability to find a particle at radius $r_f + dr_f$, that before core collapse was at radius r_i with velocity $\mathbf{v}_i(r_i)$ is

$$P(r_f|\mathcal{E}_i, L)dr_f = \frac{2d\tau}{T(\mathcal{E}_i, L)} = \frac{2}{T(\mathcal{E}_i, L)} \frac{dr_f}{\sqrt{\mathcal{E}_f^2 - \mathcal{V}_{\text{eff}}^2(r_f, L)}} \quad (\text{B1})$$

where T is the orbital period. The change in energy is given by the condition $\mathbf{v}_i(r_i) = \mathbf{v}_f(r_i)$, that in GR, for

the radial component becomes

$$\mathcal{E}_f^2 = \mathcal{E}_i^2 + \mathcal{V}_{\text{eff},f}^2(r_i, L) - \mathcal{V}_{\text{eff},i}^2(r_i, L) \quad (\text{B2})$$

The final distribution density is thus obtained by integrating the initial density weighted by this probability

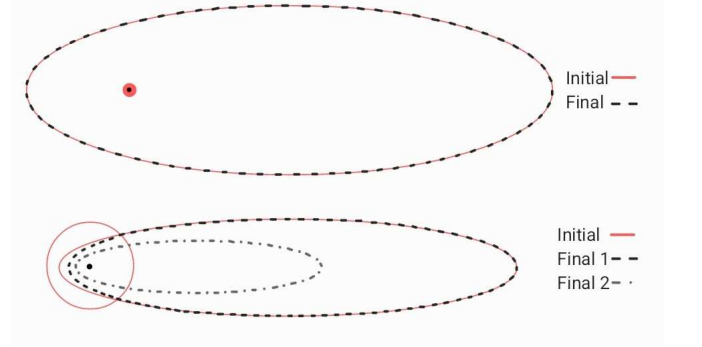


FIG. 9. Illustration of the orbital change when the critic core collapses to a SMBH. There are two cases for the initial state of the DM particle. Top: the initial DM particle orbits entirely outside the critic core (solid red). When the collapse occurs, its energy and therefore its orbit, remain unchanged (dashed black). See in figure 8, the gravitational potentials are identical outside the core radius. Bottom: the initial DM particle has its pericenter inside the core (solid red circle corresponds to the core, solid red ellipse corresponds to the particle's orbit). Two possible endings result in this case. If the DM particle was outside the core at the moment of collapse, its orbits changes slightly by reducing its pericenter (Final 1, dashed black). If on the contrary, the DM particle was inside the core at the moment of collapse, its orbits would change completely with inner pericenter and apocenter (Final 2, dotted dashed gray). However, this particle now belongs to the SMBH, and we subtract its contribution to the final DM density profile .

over the appropriate range of radius $[r_1, r_2]$ that can contribute to the particle being located at radius r_f after collapse

$$\rho(r_f) = \frac{1}{r_f^2} \int_{r_1}^{r_2} dr_i r_i^2 \rho_i(r_i) P(r_f|r_i, \mathbf{v}_i) \quad (\text{B3})$$

To find $[r_1, r_2]$ for every r_f , we need the explicit dependence on \mathcal{E}_i and L . This results in computing the triple integral

$$\rho(r_f) = \frac{4\pi m^4}{r_f^2} \int dL d\mathcal{E}_i dr_i \frac{L \mathcal{E}_i P(r_f|\mathcal{E}_i, L) f_i(\mathcal{E}_i, L)}{[g_{00}(r_i)(\mathcal{E}_i^2 - \mathcal{V}_i^2(r_i, L))]^{1/2}} \quad (\text{B4})$$

Additionally, we require that no particle inside the core at the moment of collapse, can contribute to the final density, as it will become part of the SMBH. We impose $r_1, r_2 \geq R_c$. For the case studied in this work, the critic core of 300 keV fermions has a mass and radius of $M_c = 4 \times 10^6 M_\odot$, $R_c = 9.3 [M_c]$. We compute equation B4 using `scipy.integrate.tplquad`.

- [1] P. Gondolo and J. Silk, Dark matter annihilation at the galactic center, *Physical Review Letters* **83**, 1719 (1999).
- [2] P. Ullio, H. Zhao, and M. Kamionkowski, Dark-matter spike at the galactic center?, *Physical Review D* **64**, 043504 (2001).
- [3] D. Merritt, Evolution of the dark matter distribution at the galactic center, *Physical Review Letters* **92**, 201304 (2004).
- [4] L. Sadeghian, F. Ferrer, and C. M. Will, Dark-matter distributions around massive black holes: A general relativistic analysis, *Physical Review D* **88**, 063522 (2013).
- [5] P. J. E. Peebles, Star Distribution Near a Collapsed Object, *Astrophysical Journal* **178**, 371 (1972).
- [6] P. Young, Numerical models of star clusters with a central black hole. i-adiabatic models, *Astrophysical Journal*, Part 1, vol. 242, Dec. 15, 1980, p. 1232-1237 **242**, 1232 (1980).
- [7] G. D. Quinlan, L. Hernquist, and S. Sigurdsson, Models of Galaxies with Central Black Holes: Adiabatic Growth in Spherical Galaxies, *Astrophysical Journal* **440**, 554 (1995), [arXiv:astro-ph/9407005](https://arxiv.org/abs/astro-ph/9407005) [astro-ph].
- [8] M. Hénon, L'évasion des étoiles hors des amas isolés, *Annales d'Astrophysique*, Vol. 23, p. 668 **23**, 668 (1960).
- [9] W. Dehnen, A family of potential–density pairs for spherical galaxies and bulges, *Monthly Notices of the Royal Astronomical Society* **265**, 250 (1993).
- [10] D. Merritt, M. Milosavljević, L. Verde, and R. Jimenez, Dark matter spikes and annihilation radiation from the galactic center, *Physical Review Letters* **88**, 191301 (2002).
- [11] G. Bertone and D. Merritt, Time-dependent models for dark matter at the galactic center, *Physical Review D* **72**, 103502 (2005).
- [12] G. Bertone, A. R. A. C. Wierda, D. Gaggero, B. J. Kavanagh, M. Volonteri, and N. Yoshida, Dark Matter Mounds: towards a realistic description of dark matter overdensities around black holes, [arXiv e-prints](https://arxiv.org/abs/2404.08731), [arXiv:2404.08731](https://arxiv.org/abs/2404.08731) (2024), [arXiv:2404.08731](https://arxiv.org/abs/2404.08731) [astro-ph.CO].
- [13] A. Belikov and J. Silk, Diffuse gamma ray background from annihilating dark matter in density spikes around supermassive black holes, *Physical Review D* **89**, 043520 (2014).
- [14] T. Lacroix, C. Boehm, and J. Silk, Probing a dark matter density spike at the galactic center, *Physical Review D* **89**, 063534 (2014).
- [15] A. Abramowski, F. Acero, F. Aharonian, A. Akhperjanian, G. Anton, A. Barnacka, U. B. De Almeida, A. Bazer-Bachi, Y. Becherini, J. Becker, *et al.*, Search for a dark matter annihilation signal from the galactic center halo with hess, *Physical Review Letters* **106**, 161301 (2011).
- [16] G. A. Gómez-Vargas, M. A. Sánchez-Conde, J.-H. Huh, M. Peiró, F. Prada, A. Morselli, A. Klypin, D. G. Cerdeño, Y. Mambrini, and C. Muñoz, Constraints on wimp annihilation for contracted dark matter in the inner galaxy with the fermi-lat, *Journal of Cosmology and Astroparticle Physics* **2013** (10), 029.
- [17] T. Daylan, D. P. Finkbeiner, D. Hooper, T. Linden, S. K. Portillo, N. L. Rodd, and T. R. Slatyer, The characterization of the gamma-ray signal from the central milky way: A case for annihilating dark matter, *Physics of the Dark Universe* **12**, 1 (2016).
- [18] R. Yunis, C. R. Argüelles, N. E. Mavromatos, A. Moliné, A. Krut, M. Carinci, J. A. Rueda, and R. Ruffini, Galactic center constraints on self-interacting sterile neutrinos from fermionic dark matter (“ino”) models, *Physics of the Dark Universe* **30**, 100699 (2020), [arXiv:2008.08464](https://arxiv.org/abs/2008.08464) [astro-ph.CO].
- [19] T. Lacroix, Dynamical constraints on a dark matter spike at the Galactic centre from stellar orbits, *Astronomy & Astrophysics* **619**, A46 (2018), [arXiv:1801.01308](https://arxiv.org/abs/1801.01308) [astro-ph.GA].
- [20] G. Heißel, T. Paumard, G. Perrin, and F. Vincent, The dark mass signature in the orbit of S2, *Astron. Astrophys.* **660**, A13 (2022), [arXiv:2112.07778](https://arxiv.org/abs/2112.07778) [astro-ph.GA].
- [21] R. Abuter *et al.* (GRAVITY), Mass distribution in the Galactic Center based on interferometric astrometry of multiple stellar orbits, *Astron. Astrophys.* **657**, L12 (2022), [arXiv:2112.07478](https://arxiv.org/abs/2112.07478) [astro-ph.GA].
- [22] A. Foschi *et al.* (GRAVITY), Using the motion of S2 to constrain scalar clouds around Sgr A*, *Mon. Not. Roy. Astron. Soc.* **524**, 1075 (2023), [arXiv:2306.17215](https://arxiv.org/abs/2306.17215) [astro-ph.GA].
- [23] G. Bertone and T. M. Tait, A new era in the search for dark matter, *Nature* **562**, 51 (2018).
- [24] K. Eda, Y. Itoh, S. Kuroyanagi, and J. Silk, Gravitational waves as a probe of dark matter minispikes, *Physical Review D* **91**, 044045 (2015).
- [25] X.-J. Yue, W.-B. Han, and X. Chen, Dark matter: an efficient catalyst for intermediate-mass-ratio-inspiral events, *The Astrophysical Journal* **874**, 34 (2019).
- [26] V. Cardoso and A. Maselli, Constraints on the astrophysical environment of binaries with gravitational-wave observations, *Astronomy & Astrophysics* **644**, A147 (2020).
- [27] B. J. Kavanagh, D. A. Nichols, G. Bertone, and D. Gaggero, Detecting dark matter around black holes with gravitational waves: Effects of dark-matter dynamics on the gravitational waveform, *Physical Review D* **102**, 083006 (2020).
- [28] R. Ruffini, C. R. Argüelles, and J. A. Rueda, On the core-halo distribution of dark matter in galaxies, *MNRAS* **451**, 622 (2015), [arXiv:1409.7365](https://arxiv.org/abs/1409.7365).
- [29] C. R. Argüelles, A. Krut, J. Rueda, and R. Ruffini, Novel constraints on fermionic dark matter from galactic observables I: The Milky Way, *Phys. Dark Universe* **21**, 82 (2018), [arXiv:1810.00405](https://arxiv.org/abs/1810.00405).
- [30] C. R. Argüelles, M. I. Díaz, A. Krut, and R. Yunis, On the formation and stability of fermionic dark matter haloes in a cosmological framework, *MNRAS* **502**, 4227 (2021), [arXiv:2012.11709](https://arxiv.org/abs/2012.11709) [astro-ph.GA].
- [31] A. Krut, C. R. Argüelles, P. H. Chavanis, J. A. Rueda, and R. Ruffini, Galaxy Rotation Curves and Universal Scaling Relations: Comparison between Phenomenological and Fermionic Dark Matter Profiles, *Astrophys. J.* **945**, 1 (2023), [arXiv:2302.02020](https://arxiv.org/abs/2302.02020) [astro-ph.CO].

- [32] M. F. Mestre, C. R. Argüelles, D. D. Carpintero, V. Crespi, and A. Krut, Modelling the Track of the GD-1 Stellar Stream Inside a Host with a Fermionic Dark Matter Core-Halo Distribution, [arXiv e-prints](#), arXiv:2404.19102 (2024), arXiv:2404.19102 [astro-ph.GA].
- [33] C. R. Argüelles, A. Krut, J. Rueda, and R. Ruffini, Novel constraints on fermionic dark matter from galactic observables II: Galaxy scaling relations, *Phys. Dark Universe* **24**, 100278 (2019).
- [34] E. A. Becerra-Vergara, C. R. Argüelles, and et al., Geodesic motion of S2 and G2 as a test of the fermionic dark matter nature of our Galactic core, *Astronomy & Astrophysics* **641**, A34 (2020), arXiv:2007.11478 [astro-ph.GA].
- [35] E. A. Becerra-Vergara, C. R. Argüelles, and et al., Hinting a dark matter nature of Sgr A* via the S-stars, *MNRAS* **505**, L64 (2021), arXiv:2105.06301 [astro-ph.GA].
- [36] C. R. Argüelles, M. F. Mestre, E. A. Becerra-Vergara, V. Crespi, A. Krut, J. A. Rueda, and R. Ruffini, What does lie at the Milky Way centre? Insights from the S2-star orbit precession, *MNRAS* **511**, L35 (2022), arXiv:2109.10729 [astro-ph.GA].
- [37] C. R. Argüelles, K. Boshkayev, A. Krut, G. Nurbakhyt, J. A. Rueda, R. Ruffini, J. D. Uribe-Suárez, and R. Yunis, On the growth of supermassive black holes formed from the gravitational collapse of fermionic dark matter cores, *MNRAS* **523**, 2209 (2023), arXiv:2305.02430 [astro-ph.CO].
- [38] C. R. Argüelles, J. A. Rueda, and R. Ruffini, Baryon-induced Collapse of Dark Matter Cores into Supermassive Black Holes, *APJ Letters* **961**, L10 (2024), arXiv:2312.07461 [astro-ph.GA].
- [39] R. Gilli, C. Norman, F. Calura, F. Vito, R. Decarli, S. Marchesi, K. Iwasawa, A. Comastri, G. Lanzuisi, F. Pozzi, Q. D’Amato, C. Vignali, M. Brusa, M. Mignoli, and P. Cox, Supermassive black holes at high redshift are expected to be obscured by their massive host galaxies’ interstellar medium, *Astronomy & Astrophysics* **666**, A17 (2022), arXiv:2206.03508 [astro-ph.GA].
- [40] D. D. Kocevski, M. Onoue, K. Inayoshi, and et al., Hidden Little Monsters: Spectroscopic Identification of Low-mass, Broad-line AGNs at $z \lesssim 5$ with CEERS, *APJ Letters* **954**, L4 (2023), arXiv:2302.00012 [astro-ph.GA].
- [41] X. Fan, E. Bañados, and R. A. Simcoe, Quasars and the Intergalactic Medium at Cosmic Dawn, *Anual Review A & A* **61**, 373 (2023), arXiv:2212.06907 [astro-ph.GA].
- [42] J. L. Synge, ed., *Relativity: The General Theory* (Interscience Publishers, New York., 1960).
- [43] J. Binney and S. Tremaine, *Galactic dynamics*, Vol. 13 (Princeton university press, 2011).
- [44] P.-H. Chavanis, Statistical mechanics of self-gravitating systems in general relativity: I. the quantum fermi gas, *The European Physical Journal Plus* **135**, 1 (2020).
- [45] P.-H. Chavanis and J. Sommeria, Degenerate equilibrium states of collisionless stellar systems, *Monthly Notices of the Royal Astronomical Society* **296**, 569 (1998).
- [46] P.-H. Chavanis, Generalized thermodynamics and kinetic equations: Boltzmann, landau, kramers and smoluchowski, *Physica A: Statistical Mechanics and its Applications* **332**, 89 (2004).
- [47] P.-H. Chavanis, M. Lemou, and F. Méhats, Models of dark matter halos based on statistical mechanics: The fermionic king model, *Physical Review D* **92**, 123527 (2015).
- [48] O. Klein, On the Thermodynamical Equilibrium of Fluids in Gravitational Fields, *Reviews of Modern Physics* **21**, 531 (1949).
- [49] P.-H. Chavanis, Statistical mechanics of self-gravitating systems in general relativity: I. The quantum Fermi gas, *European Physical Journal Plus* **135**, 290 (2020), arXiv:1908.10806 [gr-qc].
- [50] J. R. Oppenheimer and G. M. Volkoff, On massive neutron cores, *Phys. Rev.* **55**, 374 (1939).
- [51] J. F. Navarro, C. S. Frenk, and S. D. White, A universal density profile from hierarchical clustering, *The Astrophysical Journal* **490**, 493 (1997).
- [52] N. Speeney, A. Antonelli, V. Baibhav, and E. Berti, Impact of relativistic corrections on the detectability of dark-matter spikes with gravitational waves, *Phys. Rev. D* **106**, 044027 (2022).
- [53] D. Merritt, Single and binary black holes and their influence on nuclear structure, arXiv preprint astro-ph/0301257 (2003).
- [54] M. H. Chan and C. M. Lee, Indirect evidence for dark matter density spikes around stellar-mass black holes, *The Astrophysical Journal Letters* **943**, L11 (2023).
- [55] K. Qin and W.-C. Chen, An alternative channel to black hole low-mass x-ray binaries: Dynamical friction of dark matter?, *The Astrophysical Journal* **971**, 57 (2024).
- [56] P. Virtanen, R. Gommers, T. E. Oliphant, M. Haberland, T. Reddy, D. Cournapeau, E. Burovski, P. Peterson, W. Weckesser, J. Bright, S. J. van der Walt, M. Brett, J. Wilson, K. J. Millman, N. Mayorov, A. R. J. Nelson, E. Jones, R. Kern, E. Larson, C. J. Carey, Í. Polat, Y. Feng, E. W. Moore, J. VanderPlas, D. Laxalde, J. Perktold, R. Cimrman, I. Henriksen, E. A. Quintero, C. R. Harris, A. M. Archibald, A. H. Ribeiro, F. Pedregosa, P. van Mulbregt, and SciPy 1.0 Contributors, SciPy 1.0: Fundamental Algorithms for Scientific Computing in Python, *Nature Methods* **17**, 261 (2020).